Volume 1 | Number 1 | Jan 2013 | Pages 1–100

Journal of
Materials Chemistry A

Materials for energy and sustainability
www.rsc.org/materialsA

Li⁺

ROYAL SOCIETY
OF CHEMISTRY

ROYAL SOCIETY
OF CHEMISTRY

www.rsc.org/materialsA

Graphical Abstract

A novel Cu@ZnO core-shell nanobrushes exhibit high-performance photocatalytic selectivity-degradation for polycyclic aromatic hydrocarbons (PAHs) under UV-light irradiation.

Journal Name

ARTICLE
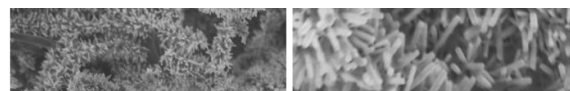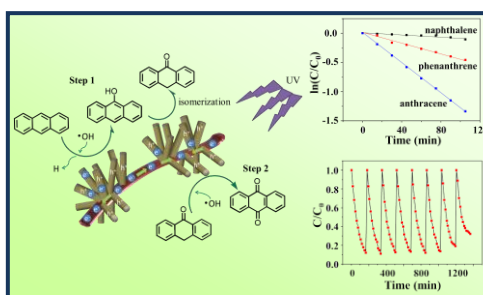
Construction of Cu@ZnO Nanobrushes Based on Cu Nanowires and Their High-performance Selectivity-degradation for Polycyclic Aromatic Hydrocarbons

Hanxing Chen, Ming Wen,[*] Zaidi Huang, Qingsheng Wu,[*] Jiali Liu and Teng Tu

Highly active Cu@ZnO brush-like nanostructures have been successfully synthesized through the heteroepitaxial growth process of ZnO branched nanorods (NRs) based on Cu core nanowires (NWs), and used for the evaluation of selective catalytic degradation for polycyclic aromatic compounds. The resultant Cu@ZnO nanobrushes, with the main diameter of ~ 500nm, consist of Cu core NWs with diameter of ~50 nm and outer ZnO branch NRs shells with thickness of ~250nm. As-designed Cu@ZnO nanobrushes exhibit high-performance for the selective catalytic degradation of polycyclic aromatic compounds. Nearly 90% conversion with the reaction rate constant (k) of 0.012 min^{-1} can be achieved for anthracene, while only about 50% and 10% conversions are shown for phenanthrene and naphthalene, respectively. Besides the high efficient transportation of electron, Cu NWs have strong capacity for oxygen activation which results in the gathering of negative charges and rich chemisorbed oxygen onto the surface, it can be responsible for high catalytic efficiency of Cu@ZnO nanobrush toward the selectivity degradation of anthracene for polycyclic aromatic hydrocarbons.

1. Introduction

The fabrication of heterostructured metal-semiconductor nanomaterials have attracted great research interest due to their unique advanced optical, electrical, magnetic and catalytic properties, which endow these hybrid materials with novel unprecedented functions or enhanced performances.[1,2] Much research work has been devoted to the delicate combination of a variety of metal–semiconductor nanomaterials with complex structures in multiple dimensions, such as Hg@ß-HgS,[3] Ag@ZnO,[4] Au@CdSe,[5] Au@CdS,[6] Au@PdS,[7] etc. for their potential applications in solar-energy conversion, microelectronics, photocatalysis, and so on.[8] Furthermore, the incorporation of one-dimensional (1D) nanoscaled building blocks of metal and semiconductor into integrated heterostructured photocatalysts benefits to get highly efficient separation and transfer of photoinduced charges.[9-11] Especially, the multiple dimensions hierarchical metal–semiconductor nanostructures can induce well performance for the reaction, which is a result of the existence of fertile catalytically active sites and greatly facilitating of reactant diffusion and transport in large amount of macropores.[12-21] But the synthesis of 1D hierarchical structured metal-semiconductor nanophotocatalysts with large specific surface area has not been well controlled yet. Meanwhile, few research works about economical metal-semiconductor with high catalytic-selectivity and high electron transportation rate has been reported.

On the other hand, polycyclic aromatic compounds are a class of persistent organic pollutants of special concern,

because they are carcinogenic and mutagenic compounds. All polycyclic aromatic compounds are neutral and nonpolar compounds, and have high stability. They are great difficulty to be degraded.[22-24] All of them have high melting point, low vapour pressure and water solubility. Photolysis is one of the major transformation processes affecting the fate of polycyclic aromatic compounds in the aquatic environment. Sunlight photo alteration processes are well known to play an important role in the degradation of polycyclic aromatic hydrocarbons (PAHs) by generation of highly reactive intermediates, mainly including hydroxyl radical (-OH), a powerful non-specific oxidant. Environmental applications of nanoscaled photocatalysts, especially the nano-semiconductor of ZnO and TiO$_2$, have been extensively investigated to treat such organic pollutants. By employing TiO$_2$ as photocatalysts, Navarro group has examined the photooxidative degradation of mixture of six PAHs, which were actually extracted from oil-contaminated soil samples in triethylamine/water mixed solvent, by using ZnO/Na$_2$S$_2$O$_8$ system with high surface areas under UV irradiation.[22] But to date, the degradation for polycyclic aromatic compounds by present semiconductor nano-photocatalysts still has not been so efficient due to the low electron-hole pair transportation.[25-31] Using metal to enhance the electron mobility is a good way to solve this problem.

In this paper, Cu@ZnO brush-like hetero-nanostructures have been successfully synthesized via the heteroepitaxial growth process of ZnO branched nanorods (NRs) based on Cu

nanowires (NWs). The investigation results indicated that as-obtained Cu@ZnO nanobrushes exhibit high-performance selective-catalytic-degradation of anthracene for PAHs, due to the hierarchical brush-like nanostructures and the synergistic effect between metal Cu NWs and ZnO NRs as well as the (001) plane-dominant surface of ZnO NRs which are attractive for highly efficient photocatalysis.

2. Experimental section

2.1. Chemicals

Glucose ($C_6H_{12}O_6$, 99.5%), 1-Hexadecylamine (HDA, 90.0%), Copper(II) chloride dihydrate ($CuCl_2 \cdot 2H_2O$, 99.0%), Polyvinylpyrrolidone K-30 (PVP, $(C_6H_9NO)_n$, Mw=40000), hexamethylenetetramine (HMT, $C_6H_{12}N_4$, 99.0%), zinc nitrate hexahydrate ($Zn(NO_3)_2 \cdot 6H_2O$, 99.0%), Zinc acetate dehydrate ($C_4H_6O_4Zn$, 99.0%), Naphthalene ($C_{10}H_8$, 99%), Phenanthrene ($C_{14}H_{10}$, 95%), Anthracene ($C_{14}H_{10}$, 98%) were purchased from Aladdin Chemical Reagent Co., Ltd., Ethyl Alcohol (C_2H_6O, 99.5%), Potassium Hydroxide (KOH, 90%), Methanol (CH_4O, 99.5%) were purchased from Sinopharm Chemical Reagent Co., Ltd. All the reagents were analytical purity and used without further purification.

2.2. Preparation of Cu nanowires

In a standard synthesis, 21 mg $CuCl_2 \cdot 2H_2O$, 50 mg glucose, 180 mg HDA, and 10 mL water were mixed in a glass vial, capped, and the final solution was magnetically stirred at room temperature for 24 hrs. The vial was then transferred into an oil bath and heated at 110 ℃ for 6 hrs under magnetic stirring.[1] As the reaction proceeded, the solution gradually changed its color from blue to red-brown, implying the formation of Cu^0 species due to the reduction of Cu^{2+} by glucose. Then, the obtained Cu NWs were dispersed in the 0.1g/L PVP solution (2.5×10^{-6} M) for 4 hrs to enhance the Cu NWs adsorption capacity of ZnO nanoseeds.

2.3. Synthesis of ZnO seed solution

ZnO sol-gel solution was prepared as reported previously.[16] 125 mL zinc acetate dehydrate solution in ethyl alcohol (0.01 M) was prepared under vigorous stirring at 60 ℃. Then, 65 mL KOH solution in ethyl alcohol (0.03 M) was injected dropwise into the above solution. The sol-gel solution of ZnO seeds was obtained after continuous stirring at 60℃ for 2 hrs.

2.4. Synthesis of Cu@ZnO nanobrushs

The obtained Cu NWs were dispersed in the prepared ZnO seed solution. After 4 hrs stirring, the obtained ZnO seed-coated Cu NWs suspension was suspended in a 10 mL aqueous solution composed of equimolar zinc nitrate (5×10^{-5} mol) and HMT (5×10^{-5} mol). After incubation at 85℃ for 6 hrs and , the system was cooled to room temperature, the resulting product was removed from the solution, rinsed thoroughly with deionized water and ethyl alcohol in several times, followed the drying treatment under vacuum for further characterization.

2.5. Characterization

The size and morphology of the as-prepared products were examined by a HITACHIS-4800 (Japan) Field-emission scanning electron microscopy (FE-SEM), a JEM-2100 (Japan) transmission electron microscopy (TEM), high-resolution transmission electron microscopy (HRTEM) and selected-area electron diffraction pattern (SAED), respectively. Element analysis was measured by energy dispersive X-ray spectroscopy (EDS) conducted at 20 keV on an EMAX X-act EDS instrument (Horiba). The powder X-ray diffraction analysis (XRD) patterns were characterized by Bruker D8 (German) diffractometer with a Cu Kα X-ray radiation source (λ= 0.154056 nm). X-ray Photoelectron Spectroscopy (XPS) experiments were carried out on an Axis Ultra DLD system (Shimadzu) using Al K radiation (hγ=1486.6 eV). The whole spectra (0~1200eV) and the narrow spectra of all the elements with much high resolution were both recorded by using RBD 147 interface (RBD Enterprises, USA) through the AugerScan 3.21 software. Binding energies were calibrated by using the containment carbon (C1s=284.6eV). The specific surface areas of the samples were determined through nitrogen adsorption at 77 K on the basis of BET equation using a Micromeritics ASAP 2020 V3.00 H.

2.6. Photocatalytic Test

We have compared the photooxidation ability of the as-prepared materials Cu nanowires and Cu@ZnO nanobrushes. The photocatalytic activities of the prepared catalysts were evaluated by the degradation of polycyclic aromatic compounds (naphthalene, phenanthrene and anthracene) which are a class of persistent organic pollutants of special concern because they are carcinogenic and mutagenic compounds.[22-24,29-32] The photocatalytic tests were performed in a reactor equipped with a cooling water-cycle system to keep the temperature stable. A 500W xenon lamp was used as the light source. In a typical UV-light photocatalytic experiment, 10 mg of the catalyst was dispersed in 50 mL naphthalene, phenanthrene and anthracene (50 μg•L^{-1}) methanol solution separately, and the obtained suspension was magnetically stirred in the dark for 1 hr to achieve adsorption-desorption equilibrium. During illumination, 3 mL of the suspension was withdrawn periodically from the reactor chamber, followed by centrifugation and filtration, and the obtained clear solution was analyzed by ultraviolet spectroscopy (8453 UV/VIS, Agilent). The degradation rate of polycyclic aromatic compounds was calculated by the following equation: $C/C_0=A/A_0$ and $\ln(C/C_0)=\ln(A/A_0)$, where C_0 and A_0 separately stands for the initial concentration of polycyclic aromatic compound solution and initial absorbance of solution; C and A separately stands for the concentration of polycyclic aromatic compound solution after xenon lamp irradiation and absorbance of solution at any time. Furthermore, high performance liquid chromatography (HPLC) is used to characterize the componentsof products which are catayized by materials, on Varian 210 instrument (USA).
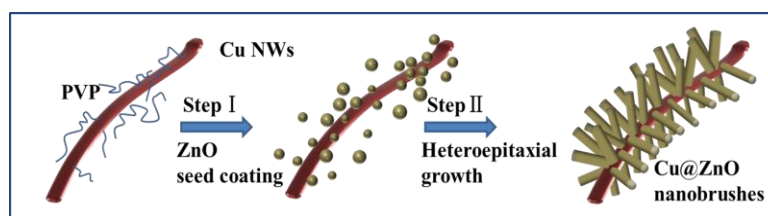
Scheme 1. A schematic illustration of the procedure for the controllable synthesis of the Cu@ZnO nanobrushes based on Cu core NWs assemblies via the seed growth approach.

3. Results and Discussion

3.1. Mechanism of Fabrication

   Controlling synthesis of Cu@ZnO brush-like nanostructures was carried out through the heteroepitaxial growth of ZnO branched NRs based on Cu core NWs via bottom up process in solution, and was illustrated in Scheme 1.[4,13] Firstly, PVP was used as surfactant to enhance the surface activity of Cu NWs and further lower the surface energy, in this procedure, the vinyl and the pyrrolidone of PVP molecules are oleophylic and hydrophilic, respectively. The PVP molecules can be adsorbed along them through the attractive force between their vinyl groups and lipophilic groups of the residual HDA molecules on Cu NWs, on the other side, the pyrrolidone of PVP molecules can attract ZnO nanoseeds through the attractive force between them. PVP molecules integrated Cu NWs and ZnO nanoseeds to form a unified phase, and the surface tension is decreased with the surface energy is further lowered.; after most PVP was rinsed by ethyl alcohol, the residual functional PVP molecules were left on the surface of Cu NWs, which results in the surface adsorption process of ZnO nanoseeds along the axial direction of Cu NWs (Scheme 1, Step I). In this step, the surface of Cu NWs just acts as the non-planar substrate and the adsorbed ZnO seeds on Cu NWs play a basic role as the starting sites in the following hierarchical assemblies process.[17,18] Then, the as-obtained ZnO seed-coated Cu NWs were dispersed in aqueous solution composed of equimolar zinc nitrate and HMT, followed by the heteroepitaxial growth of ZnO branched NRs on the surface of Cu core NWs to form Cu@ZnO heterostructured nanobrushes (Scheme 1, step II). During the growth process, homogeneous nucleation of ZnO seeds requires a higher activation energy barrier, and therefore, hetero-nucleation will be promoted and will be energetically more favorable. In fact, the interfacial energy between ZnO nanocrystals and Cu NWs is usually smaller than the interfacial energy between ZnO crystals and solutions.[4,13] Consequently, hetero-nucleation takes place at a lower saturation ratio onto a substrate than in homogeneous

Table 1. Surface properties of Cu@ZnO nanobrushes.

Properties	Cu@ZnO
BET surface area	80.7 m^2g^{-1}
Total pore volume (single point)	0.215 cm^3g^{-1}

solution. So epitaxial crystal growth occurs from substrate-generated nuclei arrange along the easier direction of crystallization. Because of the high concentration of precursors, a condensed phase of single-crystalline ZnO NRs perpendicular to Cu NWs surface can be obtained. As expected, well-aligned single-crystalline hexagonal NRs of typically ~50 nm in diameter showing well-defined crystallographic faces are grown along the perpendicular to the axial direction of Cu NWs and arranged in uniform arrays. In our work, Cu NWs were prepared under different reaction temperatures as well as ZnO nanoflowers directly grow from the growth solution in the absence of Cu NWs as the non-planar substrates and ZnO nanoseeds as the starting sites. We also observe the morphology of ZnO seed-coated Cu NWs during the process of the whole fabrication. ZnO nanoseeds can load on the surface of Cu NWs densely for the next hierarchical assemblies. They are shown in Figure S1-S3.

3.2. Morphologies and Structures

   The SEM and TEM images as well as BET curves of the Cu@ZnO nanobrushes are shown in Figure 1. The products are nanobrushes shaped with main diameter of ~ 500 nm (Figure 1A and B), in which ZnO branched NRs (250×50 nm) perpendicular to the axial direction of Cu NWs and arranged in uniform arrays. A distinct morphology of heteroepitaxial grown ZnO NRs with the diameter of ~ 50 nm also can be observed in TEM image in Figure 1 C. During the heteroepitaxial growth of ZnO nanorods (NRs) on the surface of Cu nanowires (NWs), amount of ZnO nanoparticles were generated from the growth solution which also acts as the solvent of the reaction system. The energy transfer and the
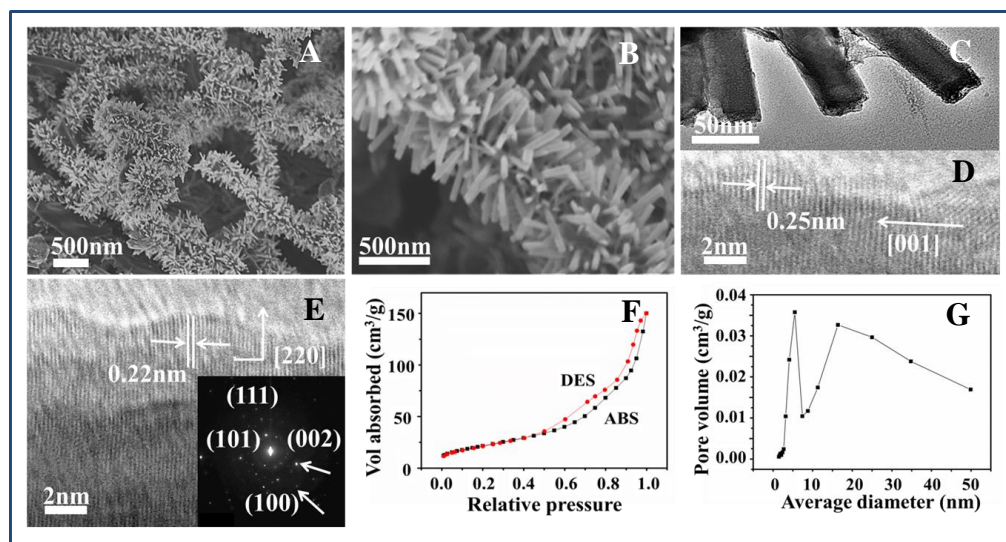

Figure 1. A-B) SEM image of Cu@ZnO nanobrushes; C) TEM image of the ZnO nanorods grow on Cu nanowire of a single nanobrush; D) HRTEM image of ZnO nanorod grows on Cu nanowire; E) HRTEM image of interface of ZnO NR and Cu NW with inset SAED; F) Absorption and desorption curve of Cu@ZnO nanobrushes and G) Pore distribution curve of Cu@ZnO nanobrushes.
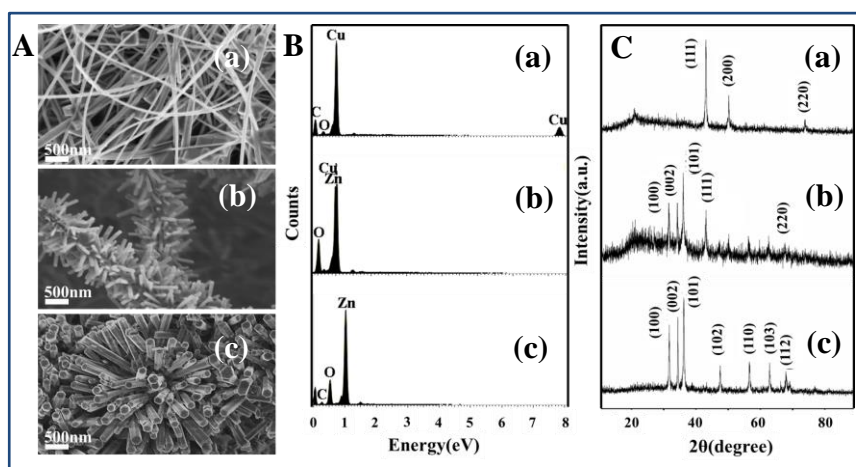
Figure 2. SEM images A), EDS B), and XRD patterns C) of Cu NWs (a), Cu@ZnO nanobrushes (b) and ZnO nanoflowers (c).

bond force between ZnO and Cu will broke part of Cu-Cu bonds in Cu nanowires which results in the breakage of Cu NWs. In addition, Cu NWs will divide into shorter ones during the ultrasonic washing process of products affected by the outer high energy force. In Figure 1D, HRTEM image of ZnO branched NRs present the crystalline structure with lattice spacing of 0.26 nm corresponding to (002) facet, which indicates that the ZnO NRs grow along [001] direction perpendicular to (002) facet. In order to understand the heterostructure crystalline, the HRTEM image of the interface between ZnO and Cu is characterized and presented in Figure E. It can be observed that the facet fringe with 0.21 nm crystalline plane spacing is assigned to the Cu {111} planes and their growth direction is along the [220] direction. SAED pattern in the inset of E recorded from the interface of ZnO and Cu indicates a mixture of the Cu [110] zone diffraction and the ZnO [1210] zone diffraction. The mixed diffraction, which exhibits the combination of hexagonal wurtzite crystal and single crystalline, is attributed to the ZnO crystal nucleus attached on the surface of the Cu NW. In the fabrication process, the reaction conditions including the different heating temperatures, the concentration of ZnO growth solution, and Cu/ZnO mole ratio all have been respectively investigated, and shown in Figure S4-S6 in Electronic Supplementary Information (ESI). Additionally, the surface area of the catalyst is also a very important factor influencing the catalytic activity. The surface area of Cu@ZnO nanobrushes was determined using the nitrogen-gas adsorption method. The absorption and desorption curve and pore distribution curve are shown in Figure 1F and G to illustrate the surface information of materials. The BET surface area and total pore volume of Cu@ZnO are summarized in Table 1. It indicates that the as-fabricated Cu@ZnO nanobrushes have high BET surface area of 80.7 $m^2 \cdot g^{-1}$ which can lead to the efficient activity of photocatalysis. From the adsorption and desorption curve, when the relative pressure (P/P_0) reaches maximum about 150 mL, the total pore volume of materials can be calculated through equation of 150*0.001547=0.23205 mL (0.001547 equals to the volume after 1 mL nitrogen gas cohesion). And the measured total pore volume is 0.215 cm^3, which is almost the same with the calculated value. In addition, Dubinin-Radushkevich and Dubinin-Astakhov analysis was used to confirm the surface adsorption and desorption information, as shown in Figure S7. It can be obviously observed that the curve can be classified into N1 hysteresis

loop class defined by International Union of Pure and Applied Chemistry (IUPAC).[33]

Figure 2 exhibits the morphologies of Cu NWs, Cu@ZnO nanobrushes and ZnO NRs together with their corresponding EDS analysis and the XRD patterns. In Figure 2B, the EDS analysis of Cu NWs (trace (a)) shows dominant Cu element and that of Cu@ZnO nanocomposites (trace (b)) shows the existence of Cu, Zn, and O elements and reveals that the Zn/O atomic ratio to be 3:1 due to the oxygen vacancy of its crystal imperfection, ZnO is the non-stoichiometric compound. Then, trace (c) gives the atomic ratio of Zn:O=3:1 for ZnO NRs, which agrees well with the target element structure. In Figure 2C, the XRD pattern of Cu NWs (trace (a)) shows three broad halos of (111) at 43.3°, (200) at 50.5°, (220) at 74.1°, respectively, which agrees well with the face centered cubic (fcc) lattice of Cu NWs (JCPDF#65-9026). Trace (c) reveals the hexagonal close packed (hcp) lattice for ZnO NRs (JCPDF#65-3411) with the corresponding peaks of (100) at 31.8°, (002) at 34.4°, (101) at 36.3°, (102) at 47.5°, (110) at 56.6°, (103) at 62.9° and (112) at 67.9°. The XRD pattern of as-prepared Cu@ZnO nanobrushes is shown in trace (b) and it matches to the mechanical superposition of Cu patterns and ZnO patterns, confirming the fabrication hierarchical heterostructured Cu@ZnO nanobrushes.

In order to further identify and compare the chemical states of elements in the architecture of Cu@ZnO nanobrushes, XPS was applied to the prepared products. The analysis spectrum for the surface of Cu NWs and Cu@ZnO nanobrushes is
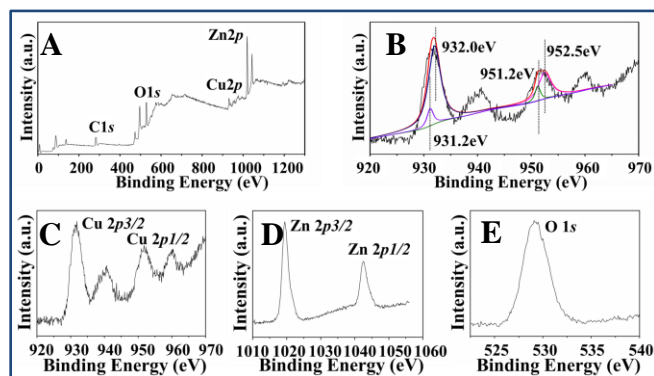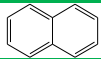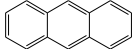

Figure 3. XPS analysis of Cu@ZnO nanobrushes (A), separated analysis of Cu 2p (B), and detailed spectra of Cu 2p (C), Zn 2p (D) and O 1s (E)

presented in Figure 3, in which the numbers of emitted photoelectrons are given as a function of binding energy up to 1100 eV. The emission from the inelastic collisions of photoelectrons gives rise to a general background. It can be observed that the Cu@ZnO nanobrushes present four photoemission peaks (Zn2p, Cu2p, O1s and C1s) in Figure 3 A. In order to clarify the exact bonding form of Cu in the products, we use XPSPEAK41 to analyze the Cu spectra. As shown in Figure 3 B, the peak of Cu 2p2/3 can be splitted to two peaks as chemical bonding of Cu-Cu bond with different crystal structure and the peak of Cu 2p1/2 can be splitted to two peaks as chemical bonding of pure Cu components and Cu-Zn bond. Magnified Cu 2p peaks in Figure 3 C, which consist of two sharp peaks at 931.81 eV and 951.86 eV, are due to the spin-orbit splitting of 2p 3/2 and 2p 1/2, respectively. The spin-orbit doublet splitting value of the 2p level, corresponding to the differences of binding energies (BE) between 2p 3/2 and 2p 1/2, was estimated to be 20.05 eV, indicating that Cu(0) is dominant. Magnified Zn 2p peaks in Figure 3 D, two peaks resulted by the 2p electrons multiple-splitting are 2p 3/2 and 2p 1/2 with BE values of 1019.4 eV and 1042.7 eV, implying for Zn(II). In addition, the O 1s peak of 529.8 eV implied that O species existed as Zn-O bond. In the Binding Energy Lookup Table for Signals from Elements and Common Chemical Species, C1s =285.0 eV, Cu2p 1/2=952.0 eV, Cu2p 3/2 =923.5 eV, Zn2p 1/2=1045.1 eV, Zn2p 3/2 =1021.4 eV, and O1s =530.0 eV. The signals of metallic bonding energy in as-obtained Cu@ZnO nanobrushes are slightly shift. The reason is suggested to be that the environment of Cu and ZnO in Cu@ZnO nanobrushes is different from pure copper and zinc oxide, and the further synergistic effect results in the signals shift of metallic bonding energy.

Table 2. Chemical structures of catalysed PAHs

PAHs	Chemical Structure	$Ln(C/C_0)$ (min^{-1})
naphthalene		0.0011
phenanthrene		0.0047
anthracene		0.012

3.3. Selective-Catalytic activities of degradation

The selective-catalytic-degradation performances of as-prepared Cu@ZnO nanobrushes are evaluated toward the photo-oxidation of PAHs including naphthalene, anthracene, and phenanthrene (as shown in Table 2) in the methyl alcohol aqueous solution, which is a typical organic carcinogenic and mutagenic pollutant in the environment.

In order to exclude the possibility that the degradation of PAHs was caused by the UV-light irradiation, the blank experiment was carried out where only selected PAHs without any photocatalyst was irradiated under UV-light (ESI, Figure S8). It can be clearly observed that the irradiation does not degrade naphthalene, phenanthrene, and anthracene in the absence of catalysts. In Figure 4A and B, when Cu@ZnO nanobrushes are involved in the reaction system, nearly 90% conversion can be achieved for anthracene, while only about 50% and 10% conversions are shown for phenanthrene and naphthalene, respectively. It exhibits the selectivity of the
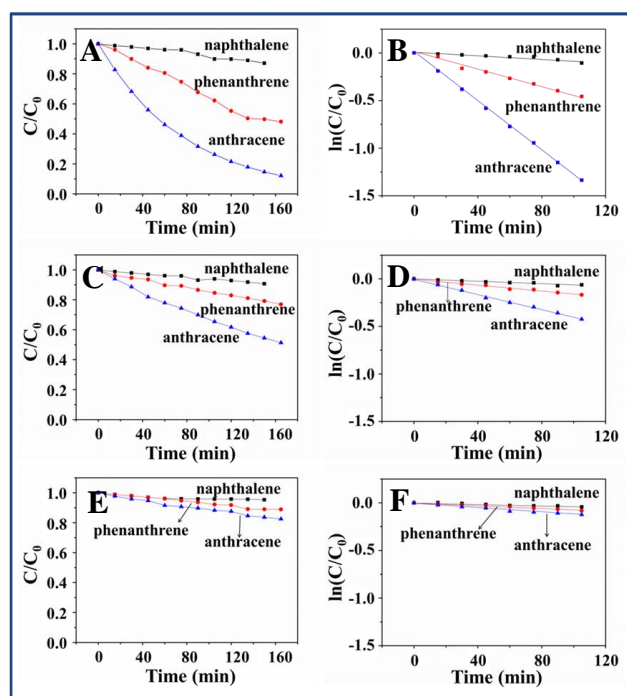

Figure 4. Plots of C/C_0 and $ln(C/C_0)$ versus time for the photocatalytic oxidation of naphthalene, phenanthrene and anthracene using as-prepared nanocatalysts of Cu@ZnO nanobrushes (A, B), ZnO nanorods (C, D) and Cu nanowires (E, F) under UV-light at r.t..

catalysts which prefers to catalyze anthracene due to its more aromatic rings and different π bond structures. So the selective photocatalytic performance toward anthracene is the highest one. This can be suggested that the interaction between benzene rings can affect the sensibility of UV light and the transportation of electrons. And isomerization can change the hybrid orbital structure; further change the response to UV light. Furthermore, more benzene rings can enhance the delocalized extent of π electron cloud, which results in the instability of molecules. On the other hand, according to frontier molecular orbital theory, the energy level of highest occupied molecular orbital (HOMO) can reflect the ability of donating electron while the energy level of lowest unoccupied molecular orbital (LUMO) can reflect the ability of gaining electron. So the different value of energy level (ΔE) between HOMO and LUMO can reflect the stability of molecules and higher ΔE corresponds to higher stability. From the authoritative statistic calculated by density functional theory, ΔE of naphthalene is higher than that of phenanthrene and anthracene which indicates that naphthalene is more stable than phenanthrene and anthracene. In other words, the added benzene ring gives phenanthrene and anthracene more delocalized π electrons and leads to higher delocalized extent, and these electrons can be activated more easily while few delocalized π electrons of naphthalene can be activated under the irradiation of UV-light. Therefore, when naphthalene is catalyzed by Cu@ZnO nanobrushes, there are much fewer flowed activated π electrons can be attacked by holes of electron-hole pairs generated in ZnO NRs. Above all, phenanthrene and anthracene could be photocatalyzed by Cu@ZnO nanobrushes but naphthalene couldn't.[34,35]

As plotted in Figure 4B, there is a good linear correlation between $ln(C/C_0)$ and the reaction time (t). It indicates that the

photodecomposition reaction of naphthalene, anthracene, and phenanthrene molecules catalyzed by Cu@ZnO catalysts can be treated as a pseudo-first-order reaction. The rate constants (k) of the photocatalytic degradation of naphthalene, phenanthrene, and anthracene over Cu@ZnO nanobrushes are determined to be 0.0011 min^{-1}, 0.0047 min^{-1} and 0.012 min^{-1}, respectively. As contrast, the photocatalytic degradation of naphthalene, phenanthrene, and anthracene over Cu NWs and ZnO NRs has also been tested respectively under same condition, and illustrated in Figure 4C-F. Their UV-vis spectra have been given in Figure S9 in ESI. It can be clear observed that the photooxidation of naphthalene, phenanthrene, and anthracene can be negligible catalyzed by Cu NWs. And the catalytic activity of ZnO NRs is unsatisfactory, which is obviously lower than that of Cu@ZnO nanobrushes.

Because the lifetime and stability are important factors for catalyst application, Figure 5 gives the recyclable oxidation of anthracene to anthraquinone catalyzed by Cu@ZnO nanobrushes under UV light at room temperature (r.t.). The catalytic activity was test over eight times. The catalysts can be successfully recycled and reused for at least seven successive cycles of reaction with conversion efficiency of around 90%. The value of k was only slightly decreased after reusing eight times. So the as-fabricated heterostructured Cu@ZnO nanobrushes have excellent stability in the catalytic oxidation of anthracene to anthraquinone. The morphologies of catalysts before the catalysis and after the fourth, eighth catalysis is shown in ESI, Figure S10.
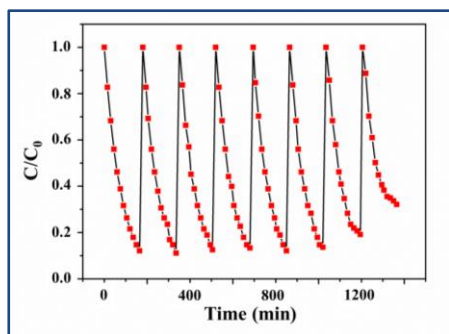

Figure 5. The recyclable oxidation of anthracene to anthraquinone photocatalyzed by Cu@ZnO nanobrushes.

Furthermore, the photocatalytic mechanism of Cu@ZnO metal-semiconductor heterostructured nanobrushes under UV-light illumination has been investigated in detail. Since Cu NWs are inert to this photodegradation reaction, obviously, the enhancement should be ascribed to the synergistic effect of Cu@ZnO hierarchical brushlike nanostructures. Because of the high conductivity of Cu NWs, Cu@ZnO heterostructures can facilitate more effective separation of photoinduced electrons and holes and reduce the charge recombination significantly due to their equilibrium band structure. Under UV irradiation, photoelectrons will transfer quickly from the surface of ZnO to Cu NWs, leaving a quantity of holes on the ZnO surface.[36-44] Especially, it is stressed here that 1D building-blocks of Cu NWs and ZnO NRs with high carrier transport property, serve as spatially extended catalysing centres' to provide direct and fast electron/hole transfer to their acceptors (CH$_3$OH, naphthalene, phenanthrene, and anthracene), which increase the chance of polycyclic aromatic
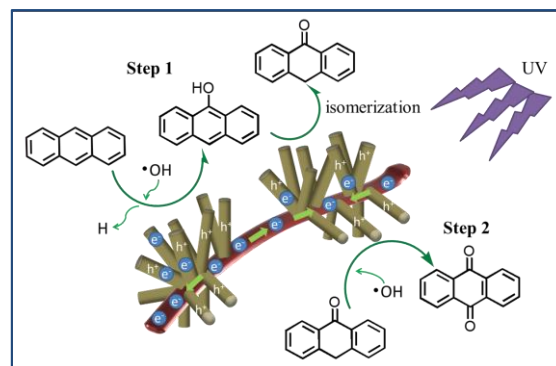
Scheme 2. The photocatalytic mechanism for the oxidation of anthracene to anthraquinone catalyzed by Cu@ZnO nanobrushes under UV-light illumination

compounds to be degraded (Scheme 2). On the other hand, the hierarchical heteroassemblies with brush structures endow the catalysts with a larger specific surface area and more accessible active sites for improved light harvesting as well as enhanced diffusion and adsorption of anthracene molecules. Moreover, as to the photocatalysis mechanism with reaction process, the oxidation mechanism of anthracene in the Cu@ZnO suspended solution under visible light irradiation is illustrated in Scheme 2. The primary rate-determining step (step 1) is initiated by the addition of OH radical generated from the solvent methyl alcohol, and then the resultant anthranol isomerizes to anthrone. The secondary step (step 2) is the formation of anthraquinone from anthrone. In this step, OH radical attack to anthrone, resulting in the formation of 9,10-dihydroxyanthracene which is further oxidized to anthraquinone on Cu@ZnO surface.[22-24] As for the catalytic product, HCLP was involved to examine final degradation products (ESI, Figure S11). The standard solution is composed by anthracene and anthraquinone with the molar ratio of 1:9 for corresponding to the target products. The spectra of catalysis reaction solution system are almost the same as that of standard solution, which proves the degradation products are composed of nearly 90% anthraquinone and 10% residual anthracene. Thus, anthracene can be successfully degraded to anthraquinone by using Cu@ZnO nanobrushes as nanocatalyst.

Conclusions

In conclusion, hetero-structured Cu@ZnO nanobrushes have been successfully constructed by the heteroepitaxial growth process of ZnO branched NRs based on Cu core NWs. Based on metals with high electrical conductivity, it gave rise to high-performance selectivity-degradation for polycyclic aromatic compounds, compared to its counterpart of Cu NWs and ZnO NRs. Such high performances arise from the synergistic effect of the hierarchical brush-like morphologies with exposed highly active (001) planes of ZnO and high specific surface area, suggesting the potential application in heterogeneous photo-nanocatalysts.

Acknowledgements

Journal of Materials Chemistry A Accepted Manuscript

Notes and references

Department of Chemistry, Key Laboratory of Yangtze River Water Environment, Ministry of Education, Tongji University, 1239 Siping Road, Shanghai 200092, R. P. China.
E-mail: m_wen@tongji.edu.cn; Fax: (+) 86-21-65981097

[1] M. S. Jin, G. N. He, H. Zhang, J. Zeng, Z. X. Xie, and Y. N. Xia, *Angew. Chem. Int. Ed.* 2011, **50**, 10560

[2] M. Rycenga, C. Cobley, J. Zeng, W. Li, C. Moran, Q. Zhang, D. Qin, Y. Xia, *Chem. Rev.* 2011, **111**, 3669

[3] L. Wu, B. G. Quan, Y. L. Liu, R. Song and Z. Y. Tang, *ACS Nano*, 2011, **5**, 2224.

[4] S. W. Wang, Y. Yu, Y. H. Zuo, C. Z. Li, J. H. Yang and C. H. Lu, *Nanoscale*, 2012, **4**, 5895.

[5] R. Costi, A. E. Saunders, E. Elmalem, A. Salant and U. Banin, *Nano Lett.*, 2008, **8**, 637.

[6] J. S. Lee, E. V. Shevchenko and D. V. Talapin, *J. Am. Chem. Soc.*, 2008, **130**, 9673.

[7] S. E. Habas, P. D. Yang and T. J. Mokari, *J. Am. Chem. Soc.*, 2008, **130**, 3294.

[8] F. Zhang, M. Wen, M.Z. Cheng, Q.S. Wu, X.G. Meng, *J. Mater. Chem.* 2010, **20**, 7661

[9] J. Perelaer, P. Smith, D. Mager, D. Soltman, S. Volkman, V. Subramanian, J. Korvink, U. Schubert, *J. Mater. Chem.* 2010, **20**, 8446

[10] J. Yang and J. Y. Ying, *Angew. Chem., Int. Ed.*, 2011, **50**, 4637

[11] A. Tao, F. Kim, C. Hess, J. Goldberger, R. R. He, Y. G. Sun, Y. N. Xia and P. D. Yang, *Nano Lett.*, 2003, **3**, 1229

[12] K. Pradel, K. Sohn, J. Huang, *Angew. Chem., Int. Ed.* 2011, **123**, 3474

[13] L. Vayssieres, *Adv. Mater.*, 2003, **15**, 5.

[14] Y. Sun, N. N. A. George, D. R. Jason, M. N. R. Ashfold, *Chem. Phys. Lett.* 2006, **431**, 352

[15] H. Gu, R. Zheng, X. Zhang, B.J. Xu, *J. Am. Chem. Soc.* 2004, **126**, 5664.

[16] C. B. Zhang, H. He, K. Tanaka, *Catal. Commun.* 2005, **6**, 211

[17] C. Pacholski, A. Kornowski and H. Weller, *Angew. Chem., Int. Ed.*, 2002, **41**, 1188

[18] Z. R. Tian, J. A. Voigt, J. Liu, B. Mckenzie, M. J. Mcdermott, M. A. Rodriguez, H. Konishi and H. F. Xu, *Nat. Mater.*, 2003, **2**, 821.

[19] L. E. Greene, M. Law, J. Goldberger, F. Kim, J. C. Johnson, Y. F. Zhang, R. J. Saykally and P. D. Yang *Angew. Chem., Int. Ed.*, 2003, **42**, 3031

[20] M. Wen, M.Z. Cheng, S.Q. Zhou, Q.S. Wu, N. Wang, L.Y. Zhou, The *J. Phys. Chem. C.*, 2012, **116**, 11702.

[21] M. Wen, Y.Z. Sun, X.M. Li, Q.S. Wu, Q.N. Wu, C.X. Wang, *J. Power Sources*, 2013, **243**, 299.

[22] N. Vela, M. Martínez-Menchón, G. Navarro, G. Pérez-Lucas, S. Navarro, *J. Photochemistry and Photobiology A: Chemistry*, 2012, **232**, 32.

[23] S. Kohtani, M. Tomohiro, K. Tokumura, R. Nakagaki, *Appl. Catal. B: Environ.* 2005, **58**, 265

[24] Z. H. Li, K. Yang, G. Liu, G. F. Deng, J. Q. Li, G. Li, R. L. Yue, J. Yang and Y. F. Chen, *Catal. Lett.* 2014, **144**, 1080

[25] C. B. Zhang, H. He, K. Tanaka, *Appl. Catal. B: Environ.* 2006, **65**, 37

[26] H. S. Kim, T. W. Kim, H. L. Koh, S. H. Lee, B.R. Min, *Appl. Catal. A: Gen.* 2005, **280**, 125

[27] H. Yoshida, Y. Yazawa, T. Hattori *Catal. Today*, 2003, **87**, 19

[28] M. M. Demir, M. A. Gulgun, Y. Z. Menceloglu, B. Erman, S. S. Abramchuk, E. E. Makhaeva, A. R. Khokhlov, V. G. Matveeva, M. G. Sulman, *Macromolecules*, 2004, **37**, 1787

[29] H. Huang, D. Y. C. Leung, D. Ye, *J. Mater. Chem.* 2011, **21**, 9647

[30] H. B. Huang, D.Y.C. Leung, *J. Catal.* 2011, **280**, 60

[31] H. Huang, D. Y. C. Leung, *ACS Catalysis*, 2011, **1**, 348

[32] M. J. Height, S. E. Pratsinis, O. Mekasuwandumrong and P. Praserthdam, *Appl. Catal. B: Environ.* 2006, **63**, 305.

[33] M. Jaroniec, L. A. Solovyov, *Langmuir*, 2006, **22**, 6757.

[34] K. R. Murphy, K. D. Butler, P. G. M. Spencer, et al. *Environ. Sci. Technol.* 2010, **44**, 9405

[35] J. H. Goldman, S. A. Rounds, J. A. Needoba, *Environ. Sci. Technol.* 2012, **46**, 4374

[36] C. Karunakaran, V. Rajeswari and P. Gomathisankar, *Solid State Sci.*, 2011, **13**, 923.

[37] M. Wen, D. Yang, Q.S. Wu, R.P. Lu, Y.Z. Zhu and F. Zhang, *Chemical Communications*, 2010, **46**, 219

[38] L. B. Hu, H. S. Kim, J. Y. Lee, P. Peumans and Y. Cui, *ACS Nano*, 2010, **4**, 2955.

[39] Y.G. Wu, M. Wen, H. Fang, Q.S. Wu, *The Journal of Physical Chemistry C,* 2014, **118**, 6307

[40] C. Yang, H. W. Gu, W. Lin, M. M. Yuen, C. P. Wong, M. Y. Xiong and B. Gao, *Adv. Mater.*, 2011, **23**, 3052.

[41] Y. G. Sun and Y. N. Xia, *Adv. Mater.*, 2002, **14**, 833.

[42] F. R. Fan, Y. Ding, D. Y. Liu, Z. Q. Tian and Z. L. Wang, *J. Am. Chem. Soc.*, 2009, **131**, 12036

[43] B.L. Sun, M. Wen, Q.S. Wu, J. Peng, *Adv. Funct. Mater.*, 2012, **22**, 2860.

[44] M. Wen, X.G. Meng, B.L. Sun, Q.S. Wu, and X.L. Chai, *Inorganic Chemistry*, 2011, **50**, 9393.